



Influence of sputtering conditions and annealing parameters on structure and morphology of NiTiO₃ ilmenite thin films

Meriem Chettab*, Quentin Simon*, Mustapha Zaghrioui, Cécile Autret-Lambert, Patrick Laffez

University of Tours, GREMAN, UMR 7347–CNRS, IUT de Blois 15 rue de la chocolaterie CS 2903, 41029 Blois Cedex, FRANCE

ARTICLE INFO

Keywords:

Nickel titanate
Radio-frequency sputtering
Thin films
Crystallographic orientation

ABSTRACT

Nickel titanate (NiTiO₃) is well known for its interesting functional properties such as photocatalysis, high-*K* materials or magnetoelectric coupling. Some of these properties are strongly dependent on crystallographic orientation and morphological characteristics. Deposition as thin films through adapted processes enables to control such feature during NiTiO₃ growth. In this context, NiTiO₃ thin films were obtained by a two-step process: *i*) room temperature radio-Frequency co-sputtering of metallic Ni and Ti targets, *ii*) *ex situ* annealing in air. Influences of the deposition and annealing parameters on the morphological and structural features of NiTiO₃ thin films were systematically studied. First, *in situ* X-ray diffraction as a function of temperature (from 30°C to 1200°C) was carried out in air on a NiTi thin film to identify suitable annealing temperatures for NiTiO₃ oxide formation. Then, effects of annealing duration and temperature on morphology and orientation were investigated. Annealing temperature was found to influence grain size, while increasing the annealing time was found to bring (006) crystallographic orientation. Finally, an increase of the deposition pressure from 0.5 Pa to 5 Pa promoted the growth of (104) oriented films with a Lotgering factor $LF_{104} = 0.44$. This approach enables to independently tune preferential orientation and grain size of NiTiO₃ thin films, by tailored deposition and annealing conditions.

1. Introduction

Nickel titanate NiTiO₃ adopts at atmospheric pressure the ilmenite rhombohedral structure with *R*3 symmetry [1]. Ilmenite structure is usually described as a derivative of the α -Al₂O₃ corundum structure in a non-primitive hexagonal unit cell. This structure is a stack of face sharing oxygen octahedrons. Two thirds of octahedral interstitial sites are occupied by alternating layers of Ni and Ti atoms along the *c* axis [2,3]. NiTiO₃ is an n-type antiferromagnetic semiconductor considered as relevant material for a wide range of technologies: photocatalysis, high dielectric constant and magnetoelectric properties. NiTiO₃ is used as a pigment for its bright yellow color [4,5]. It has also demonstrated excellent photocatalytic performances in the removal of organic pollutants from water, either as single phase [6–8] or in composite systems [9,10]. Indeed, with a band gap *E_g* lying in the range 2.2–3.2 eV [11–13], it is considered as an alternative to the well-known TiO₂ photocatalyst (*E_g* ~ 3.0 eV) in order to extend the energy harvesting from sun light toward visible radiations. Moreover its high electrical resistivity at room temperature and high dielectric permittivity make NiTiO₃ a potential candidate as high-*K* material to achieve high density data storage devices [14,15]. Finally, low temperature magnetoelectric

coupling have recently been reported on such compounds opening perspectives to design sensors or devices for data/energy processing and storage [16].

In most of the above-mentioned technologies, materials must be designed in the form of thin films to improve their life span under operating conditions or to reduce their dimensions for miniaturization constraints. NiTiO₃ thin films were grown by several techniques such as Atomic Layer Deposition [17,18], Pulsed Laser Deposition [19] and by Plasma Sputtering [6,15,20,21]. Among all these techniques, magnetron sputtering is a versatile one, suitable for the deposition of high-quality and well-adhered layers of a wide range of materials at commercially useful scales. Nonetheless, few studies were published on the influence of sputtering parameters on structural and morphological properties of NiTiO₃ thin films. Recently, Bellam *et al.* have proposed a statistical design of experiments to improve the features of NiTiO₃ thin films deposited by a Radio-Frequency magnetron co-sputtering process [21]. This statistical approach provides interesting information to evaluate, with a reduced number of experiments, the influence of large number of processing parameters (9 in their study) on the NiTiO₃ properties. However, further experiments should be required to finely tune NiTiO₃ thin films properties.

* Corresponding authors.

E-mail addresses: chettab.meriem@gmail.com (M. Chettab), quentin.simon@univ-tours.fr (Q. Simon).

<https://doi.org/10.1016/j.tsf.2020.138384>

Received 2 April 2020; Received in revised form 27 September 2020; Accepted 1 October 2020

Available online 02 October 2020

0040-6090/ © 2020 Elsevier B.V. All rights reserved.

In this context, the present study concerns the deposition of NiTiO_3 thin films by a two-step process: i) radio-frequency magnetron co-sputtering of NiTi thin films from two targets, ii) *ex situ* annealing in air to promote NiTiO_3 crystallization. This work aims to establish by a systematic approach, relationships between synthesis conditions (sputtering and annealing conditions) and resulting properties (morphological and structural) of NiTiO_3 thin films. The article is structured as follows: the influence of NiTi sputtering conditions are introduced to reach the desired stoichiometry and thickness for three deposition pressures; then, the annealing step is optimized to obtain single-phase coatings; finally the influence of the deposition pressure on the microstructural features of NiTiO_3 thin films is presented.

2. Material and methods

The experimental procedure was adapted from previous works [22,23]. Co-deposition by radio-frequency sputtering technique was used to grow NiTi thin films on silicon (100) substrates. Prior to the depositions, silicon substrates were successively cleaned in soapy water, deionized water, acetone and isopropanol. Deposition chamber was evacuated down to a base pressure of 10^{-4} Pa by combining a primary pump with a turbo molecular one. Thin films were deposited from two 2 inches metallic targets of nickel and titanium, mounted on two similar cathodes connected to their own radio-frequency power generator and tilted in a converging configuration to the substrate. Substrate to targets distance was adjusted to 9 cm. Depositions were performed under argon atmosphere with an argon flux of 25 sccm. The aperture between deposition chamber and pumping system was adjusted to regulate working pressures at 0.5 Pa, 1.5 Pa and 5 Pa. To obtain films with atomic ratio $\text{Ti/Ni} = 1$, for every deposition pressure, radio-frequency power was maintained at 30 W on Ni cathode and radio-frequency power was adjusted in the range 50–100 W on Ti target. Targets were sputtered for 30 min prior to each deposition to ensure metallic surface state. Deposition time was set between 30 and 100 min to obtain comparable thicknesses for each deposition pressure. The substrate holder wasn't heated during deposition and was connected to a rotation system to ensure uniform deposition.

After deposition, as-deposited NiTi thin films were annealed in a tubular furnace in air at atmospheric pressure. Different annealings were carried out by changing dwell temperature from 700°C to 900°C and dwell time from 1 h to 20 h. Heating and cooling rates were set to 4°C/min.

Chemical composition was determined by energy dispersive x-ray spectroscopy (EDS) with an acceleration voltage of 15 kV and a working distance of 15 mm. For each sample six positions were probed to check the homogeneity of the samples. Compositions were calculated from a deconvolution of EDS recorded spectra by Oxford Instrument AZtec. Surface morphology was examined using scanning electron microscopy (SEM, TESCAN) equipped with a Field Emission Gun operating at 10 kV. X-ray diffraction (XRD) patterns were performed in a Bruker D8 advance diffractometer, using Cu ($\text{K}\alpha_1 = 1.54056 \text{ \AA}$ and $\text{K}\alpha_2 = 1.54439 \text{ \AA}$) radiations. For the determination of NiTiO_3 synthesis temperature, Bragg Brentano $\theta-2\theta$ XRD patterns versus temperature were performed by heating from room temperature to 1200°C and recording a pattern every 50°C. Bragg Brentano scans in symmetric configuration were used to determine Lotgering factor. For phase identification, XRD patterns were measured in $\theta-2\theta$ scans with an offset of 4° to get rid of silicon peaks. Thicknesses were determined from x-ray reflectivity (XRR) measurements, recorded using a parallel X-ray beam and post-treated with the Bruker's Leptos software.

3. Results and discussion

3.1. Optimization of sputtering conditions for NiTi thin films

Changing deposition pressure affects differently deposition rates of

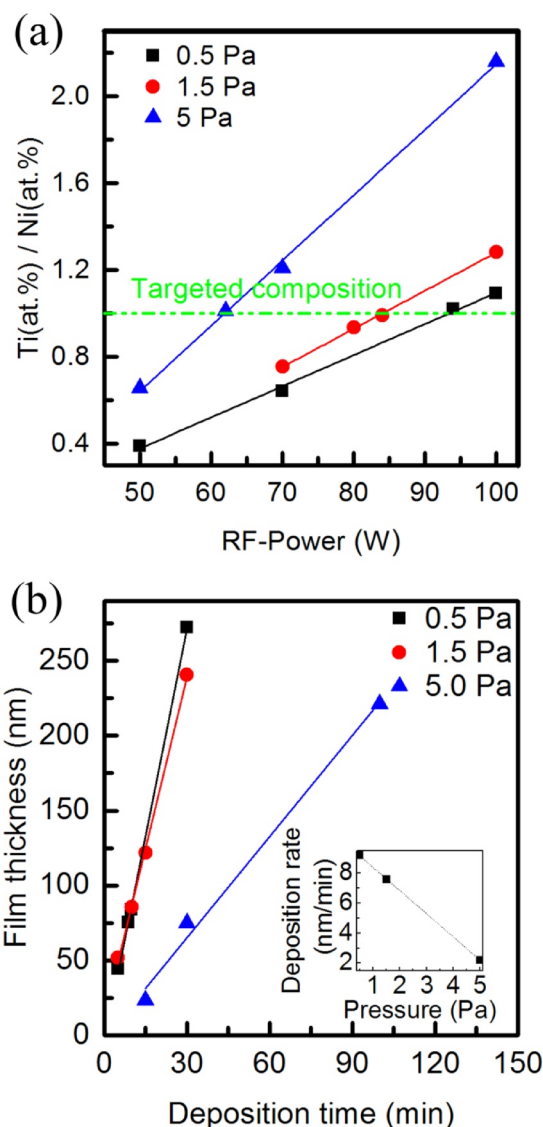


Fig. 1. (a) Ti/Ni atomic ratio as function of radio frequency (RF) power on Ti target for working pressure of 0.5 Pa, 1.5 Pa and 5 Pa. (b) Thicknesses of as-deposited NiTi thin films as function of deposition time (power applied on Ti target is 94 W, 84 W, 62 W for 0.5 Pa, 1.5 Pa and 5 Pa, respectively). Deposition rate as a function of pressure is plotted in the inset.

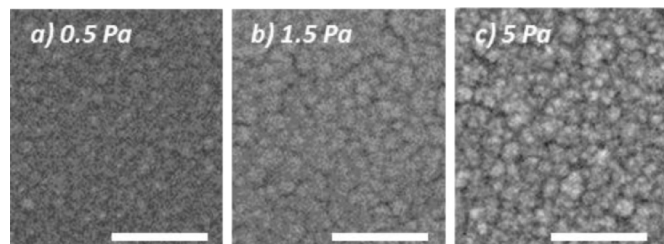
both Ni and Ti because of scattering effect and change in sputtering yield [24,25]. Hence, the key parameters to reach an atomic ratio $\text{Ti/Ni} = 1$ in multi-target co-sputtering are the radio-frequency powers applied on Ni and Ti targets. Three series of thin films were deposited at different Ar pressures (0.5 Pa, 1.5 Pa and 5 Pa). The Ti/Ni atomic ratios obtained by EDS analysis are plotted as a function of the radio-frequency power applied on Ti target while keeping radio-frequency power at 30 W on Ni target (Fig. 1(a)). For each deposition pressure, the Ti/Ni atomic ratio varies linearly with the applied radio-frequency power on titanium target. The expected composition is obtained by applying the power corresponding to the intersection between each linear fit and the dashed green line. Table 1 summarizes the optimized radio-frequency sputtering conditions to obtain stoichiometric NiTi thin films for the three deposition pressures.

One can observe that an increase of working pressure implies a change of the Ni and Ti deposition rates separately and therefore sample composition. This change is mainly related to the increase of the scattering effect of Ni and Ti atoms in different proportions. Consequently, a decrease of the radio-frequency power on Ti target is

Table 1

Optimized sputtering parameters to obtain, for every deposition pressure, stoichiometric NiTi thin films with a thickness ranging between 221 nm and 272 nm.

Pressure (Pa)	Ar flow rate (sccm)	RF power on Ti target (W)	RF power on Ni target (W)	Deposition rate (nm/min)	Deposition time (min)
0.5	25	94	30	9.2	30
1.5	25	84	30	7.6	30
5	25	62	30	2.2	100

**Fig. 2.** SEM micrographs of as-deposited samples obtained at a working pressure of 0.5 Pa, 1.5 Pa and 5 Pa during 30 min, 30 min and 100 min respectively. Scale Bar: 200 nm.

necessary to adjust the desired element stoichiometry [26].

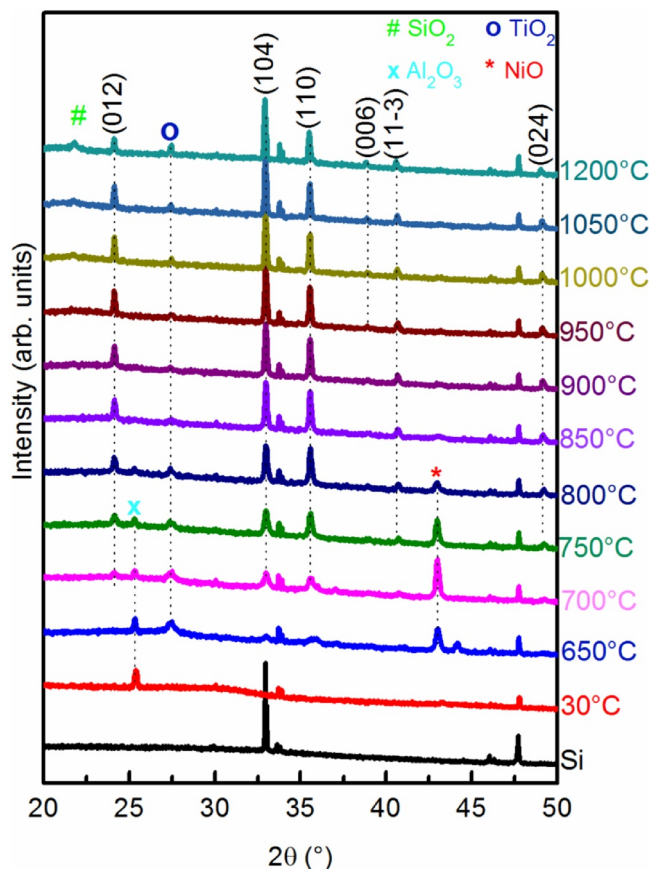
Fig. 1(b) shows thicknesses measured by XRR of as-deposited stoichiometric NiTi thin films deposited for different times and at different working pressures. Film thickness dependence on deposition time allows to calculate the deposition rate (in nm/min) by a linear regression for each pressure. The inset of Fig. 1(b) shows a decrease of deposition rate with increasing pressure. This decrease is mainly related to the increase of scattering effect that reduces the amount of Ti and Ni atoms in-coming on the substrate [27]. Table 1 gives, for every working pressure, the deposition rates and the deposited times used in the following work to obtain as-deposited films in the same range of thickness (221–272 nm).

Fig. 2 displays the SEM plan-view micrographs of optimized samples deposited at 0.5 Pa, 1.5 Pa and 5 Pa. While all the deposits are composed of very small particles, one should note that the apparent surface density evolves with deposition pressure. The microstructure changed from densely packed particles with low roughness at low pressure to porous assemblies with high roughness at high pressure. These trends are confirmed by the XRR analyses with a decrease of the critical angle and an increase of reflected signal attenuation with increasing pressure (not shown here). For instance, electronic densities calculated from critical angles are 15.6×10^{23} , 15.6×10^{23} and 11.6×10^{23} in electron per cm^3 for working pressures of 0.5 Pa, 1.5 Pa and 5 Pa respectively. This evolution of microstructure can be interpreted within the frame of the generalized structure zone diagram proposed by Anders [28], where the increase of the energy of in-coming species (at low pressure) leads to an increase in thin film density.

At this stage of the synthesis process, and for all deposition parameters, all samples are amorphous, according to XRD experiments (see part 3.2).

3.2. Optimization of annealing temperature

The optimization of the annealing step to crystallize NiTiO₃ was performed on a metallic NiTi film initially deposited at 1.5 Pa. To determine the temperature range of the annealing step, *in situ* temperature X-ray diffraction measurements were carried out (from 30°C to 1200°C with a 50°C increment) (Fig. 3). Substrate's diffraction pattern is shown by the bottom diagram on Fig. 3 for comparison. As mentioned above, the X-ray pattern at 30°C of as-deposited NiTi sample does not reveal any peaks except those of silicon substrate [29] and substrate holder made of corundum Alumina (Al₂O₃) [30]. For sake of clarity, diffractograms recorded in the range 50°C–600°C are not presented in Fig. 3. At 650°C, the sample mainly contains rutile TiO₂ [31], bunsenite

**Fig. 3.** *In situ* XRD measurement versus temperature of a stoichiometric NiTi thin film. Deposition was operated by applying 84 W on Ti target at a working pressure of 1.5 Pa during 1 h.

NiO [32] phases with traces of NiTiO₃. At 700°C, NiTiO₃ phase starts to grow significantly with appearance of diffraction peaks corresponding to (012), (104), (110) and (024) planes of the ilmenite structure in hexagonal R $\bar{3}$ symmetry (space group 148) [3]. Above 700°C, TiO₂ [31] and NiO [32] peaks tend to vanish and NiTiO₃ peaks increase in intensity. It suggests that TiO₂ and NiO phases are first formed in the samples and then react together to form NiTiO₃. These results agree with the observations of Zeng *et al.* [33]. Above 850°C, NiO is decomposed and there is still a small amount of TiO₂ left in the sample. At 950°C, NiTiO₃ crystallites with (006) oriented planes are formed in addition to the other orientations. At 1200°C, cristobalite SiO₂ (100) plane from oxidation of silicon substrate is detected [34], as also observed by Bellam *et al.* [21]. Therefore, annealing of NiTi films is conducted at temperatures ranging from 700°C to 900°C to crystallize NiTiO₃ phase without significant modification of silicon substrate.

Fig. 4(a) presents XRD patterns of thin films annealed for 1 h in air at different temperatures (700°C, 800°C and 900°C). At 700°C, the sample is composed of a mixture of NiTiO₃, NiO and TiO₂ phases. At 800°C and 900°C, a weak intensity corresponding to TiO₂ structure remains, with no evidence of NiO phase. In addition, NiTiO₃ peaks grow sharper with increasing temperature. The FWHM value of (104) and (110) diffraction peaks were similar within the same sample. These

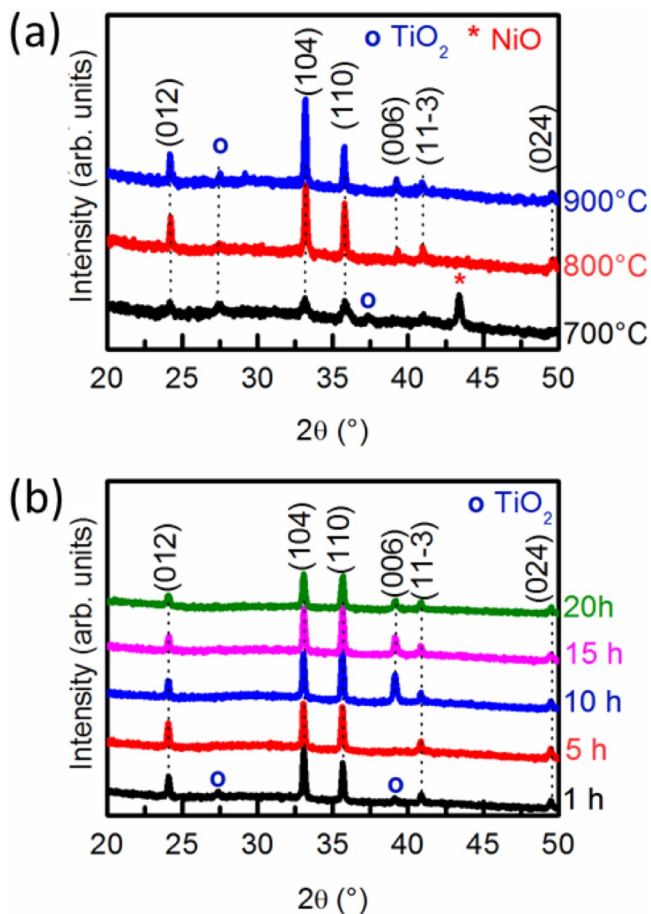


Fig. 4. (a) XRD patterns of samples deposited at 1.5 Pa and annealed for 1 h at 700°C, 800°C and 900°C. (b) X-ray diffraction patterns of NiTiO₃ films annealed at 800°C for different annealing durations.

values are: 0.5°, 0.21° and 0.18° at 700°C, 800°C and 900°C, respectively, highlighting an increase of crystalline coherence length when increasing temperature.

At this stage, as 800°C is the lower temperature allowing the formation of NiTiO₃ with a minimum of secondary phases, it is picked as annealing temperature for the remainder of the study.

The morphology of annealed samples was observed by SEM (Fig. 5). After annealing for 1 h at 700°C, (Fig. 5(a)), the film is composed of particles with two different categories of size: small (48 ± 9 nm) and larger ones (104 ± 32 nm). The small grains have the same aspect as those observed on the as-deposited NiTi films and could be a fraction of unreacted grains. The large grains may correspond to crystallized phases observed in corresponding XRD analyses (Fig. 4(a)). At 800°C, (Fig. 5(b)), grains show smooth edges with higher homogeneity in size (85 ± 26 nm) which agrees with a better crystallization of NiTiO₃. At 900°C (Fig. 5(c)), a grain growth occurs leading to a mean size of 222 ± 88 nm and sharp edges.

3.3. effect of annealing time

To obtain single phase NiTiO₃ sample, annealing was performed at 800°C for different durations. Fig. 4(b) presents XRD patterns of samples annealed at 800°C during 1 h, 5 h, 10 h, 15 h and 20 h. For 1 h, the sample is mainly composed of NiTiO₃ phase randomly oriented [3] with unreacted TiO₂ rutile phase attested by peaks at 27.34° and 39.11° corresponding to (110) and (200) rutile atomic planes [31]. This result is comparable to the pattern recorded during *in situ* XRD analyses versus temperature. When annealing time increases up to 5 h, randomly

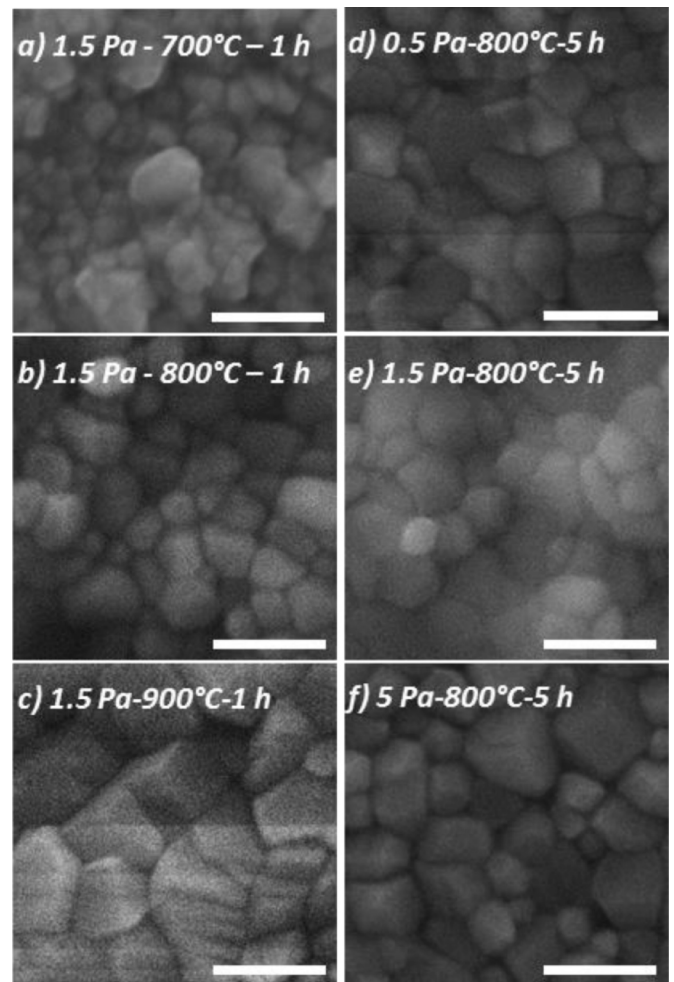


Fig. 5. SEM micrographs of samples deposited at a working pressure of 1.5 Pa and annealed for 1 hour at (a) 700°C (b) 800°C and (c) 900°C. Samples deposited at a working pressure of (d) 0.5 Pa, (e) 1.5 Pa and (f) 5 Pa and annealed at 800°C for 5 h. Scale Bar: 200 nm.

oriented NiTiO₃ ilmenite structure is solely detected with no evidence of secondary phase in the detection limit of the technique. Beyond annealing for 5 h, the samples still present single-phase ilmenite NiTiO₃ structure but with an enhancement of the (006) diffraction intensity.

The (006) intensity reaches a maximum after annealing for 10 h and then monotonously decreases for longer annealing times. Indeed, for randomly oriented powder, the (104) planes give the highest diffraction intensity with a ratio $\frac{I_{006}}{I_{104}} = 0.03$ [3]. In this study, the $\frac{I_{006}}{I_{104}}$ ratio changes from 0.6 to 0.4 and finally ends at 0.23 for 10 h, 15 h and 20 h annealing, respectively. This evolution in film preferential orientation is related to the synthesis process. The crystallization of NiTiO₃ likely initiates from top surface of the coatings from where the oxygen diffuses. Thus, for the shortest annealing durations (1 h and 5 h), the film orientation should mainly result from the reduction of surface energy between NiTiO₃ crystallites and the atmosphere along with the stress relaxation mechanism due to lattice volume change upon NiTiO₃ formation. In these conditions, no significant preferential orientation is observed. For longer annealing durations (10 h and more), the film is fully composed of oxidized NiTiO₃ and tends to organize toward a (001) preferential orientation. Beyond the stress relaxation promoted by extended annealing time, this result suggests that at this stage, the orientation of crystallite is partially re-organized from the interface between NiTiO₃ and native SiO₂ layer of the substrate. Extending the annealing time above 10 h tends to retrieve random orientation. Currently, we don't have any explanation for this phenomenon.

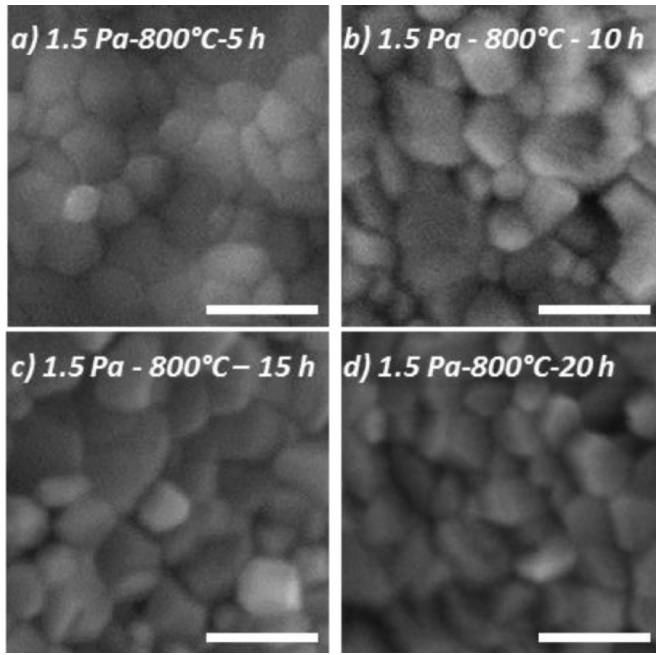


Fig. 6. SEM micrographs of samples deposited at a working pressure of 1.5 Pa and annealed during (a) 5 h (b) 10 h (c) 15 h (d) 20 h at 800°C. Scale Bar: 200 nm.

Note that experiments carried out at 700°C for 5 h (not shown here) revealed that this temperature was not high enough to enable the complete reaction of NiO and TiO₂ single oxides into NiTiO₃ in reasonable durations. These results are in agreement with data on ceramic samples from Goldman [35].

The morphologies of samples annealed at 800°C for different durations are shown in Fig. 6. For 5 h annealing (Fig. 6(a)), the surface is granular, and the mean grain size is 103 ± 26 nm. It reaches a maximum of 126 ± 38 nm at 10 h and then decreases to 104 ± 31 nm after 20 h. It is noteworthy that the maximum of grain size matches the higher intensity I_{006} of (006) diffraction peak.

3.4. Influence of working pressure

Influence of working pressure on the structure and morphology of NiTiO₃ ilmenite thin films was investigated. This parameter is well known to influence the sputtering yield of each chemical element as well as the scattering phenomena and sputtering rate. Consequently, the energy and the mobility of the in-coming species can be drastically changed, which modifies the film microstructure [24,28]. Three NiTi thin films were deposited at different pressures using deposition conditions listed in table 1. Annealing conditions are selected to obtain pure NiTiO₃ ilmenite structure for a minimum of annealing temperature and time, i.e. 800°C for 5 h. X-ray diffraction patterns of each annealed sample are showed in Fig. 7. All samples present the ilmenite phase without any trace of secondary phase [3]. However, relative diffraction peak intensities are different from those of randomly oriented powder. To quantify this deviation from random orientation of the crystallites, Lotgering factors (LF) of (104) plane are calculated for each pressure. It determines whether grains are randomly oriented (LF=0) or totally oriented (LF=1) or with intermediate preferential orientation ($0 < LF < 1$). LF is calculated from XRD intensities using the relation:

$$LF = \frac{p - p_0}{1 - p_0}$$

where $p = \frac{\sum I_{(hkl)}(nmp)}{\sum I_{(hkl)}}$ and $p_0 = \frac{\sum I_{(hkl)}(nmp)}{\sum I_{(hkl)}}$ [36] with $I_{(hkl)}$ and $I_{(hkl)}$ being the intensities of (hkl) planes of the studied sample and randomly oriented

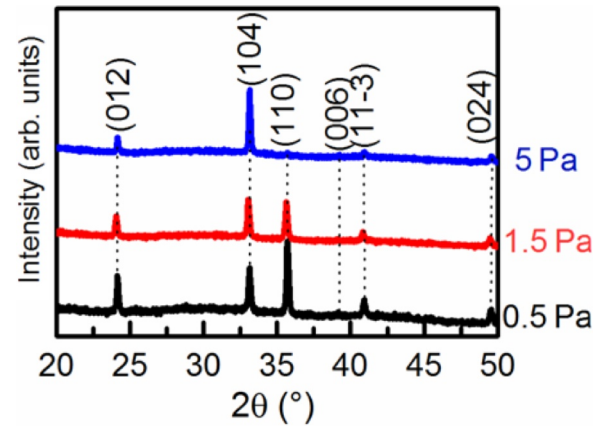


Fig. 7. : XRD patterns of NiTiO₃ samples deposited at working pressures of 0.5 Pa, 1.5 Pa and 5 Pa and annealed at 800°C for 5 h.

reference, respectively [3]. (nmp) refers to the given plane of interest, i.e. (104) plane.

At 0.5 Pa, the sample does not display significant preferential orientation. When increasing deposition pressure I_{104} increases and all other peak intensities decrease to reach a Lotgering factor $LF_{(104)} = 0.44$ for 5 Pa. Therefore, increasing deposition pressure promotes (104) phase orientation in NiTiO₃ thin films.

This evolution is likely related to the peculiar microstructure of the as-deposited NiTi coatings leading to different orientations upon the annealing step for NiTiO₃ formation. At low pressure, the dense microstructure of the NiTi films may result in high competition for preferential orientation between the stress generation/relaxation mechanisms arising from lattice volume increase upon oxidation and reduction of NiTiO₃/atmosphere surface energy. In these conditions, NiTiO₃ thin films don't present any significant preferential orientation. In a different way, the more porous microstructure for NiTi films deposited at high pressure may be characterized by lower stress generation upon oxidation that finally leads to a preferential orientation mainly governed by the minimization of surface energy between NiTiO₃ and the atmosphere. These conditions result in a thin film having a (104) preferential orientation which has been reported as being the lowest surface energy in ilmenite structure by density functional theory approaches and by atomistic simulations [37–39].

SEM observations of these samples are shown in Fig. 5. All the samples presented granular surface and a similar grain size (113 ± 28 nm, 103 ± 26 nm and 120 ± 36 nm for 0.5 Pa, 1.5 Pa and 5 Pa, respectively) with no significant differences.

3.5. Summary

In conclusion, NiTiO₃ thin films were obtained by a two-step process: a deposition of NiTi films by radio-frequency magnetron co-sputtering at various pressures (0.5 Pa, 1.5 Pa and 5 Pa) on silicon substrates followed by an annealing step in air. For every deposition pressure, an annealing at 800°C for 5 h was necessary to obtain single-phase ilmenite thin films. At 1.5 Pa, an increase of annealing time was found to promote (006) preferential orientation while an increase of temperature led to grain size increase. For an annealing treatment of 800°C for 5 h, increasing the deposition pressure tended to significantly enhance (104) crystallites orientation. This simple two-step process enabled to independently tune NiTiO₃ preferential orientation and grain size by changing the deposition pressure or the annealing temperature/time.

Funding

This work was supported by the French Ministry of Higher

Education, Research and Innovation [PhD research Grant of M. Chettab].

CRedit authorship contribution statement

Meriem Chettab: Investigation, Writing - original draft, Data curation, Formal analysis. **Quentin Simon:** Writing - review & editing, Supervision, Project administration, Funding acquisition. **Mustapha Zaghrioui:** Investigation, Writing - review & editing. **Cécile Autret-Lambert:** Investigation, Writing - review & editing. **Patrick Laffez:** Writing - review & editing, Supervision, Project administration, Funding acquisition.

Declaration of Competing Interest

None.

Acknowledgments

The authors thank Mr. Frédéric Dorvaux for help during sample deposition.

References

- [1] X. Liu, R. Hong, C. Tian, Tolerance factor and the stability discussion of ABO₃-type ilmenite, *J. Mater. Sci. Mater. Electron.* 20 (2009) 323–327, <https://doi.org/10.1007/s10854-008-9728-8>.
- [2] Tom.F.W. Barth, E. Posnjak, The Crystal Structure of Ilmenite. *Z. Für Krist. - Cryst. Mater.* 88 (1934) 265–270, <https://doi.org/10.1524/zkri.1934.88.1.265>.
- [3] R.P. Liferovich, R.H. Mitchell, Rhombohedral ilmenite group nickel titanates with Zn, Mg, and Mn: synthesis and crystal structures, *Phys. Chem. Miner.* 32 (2005) 442–449, <https://doi.org/10.1007/s00269-005-0020-7>.
- [4] J.L. Wang, Y.Q. Li, Y.J. Byon, S.G. Mei, G.L. Zhang, Synthesis and characterization of NiTiO₃ yellow nano pigment with high solar radiation reflection efficiency, *Powder Technol* 235 (2013) 303–306, <https://doi.org/10.1016/j.powtec.2012.10.044>.
- [5] G.R. Rossman, R.D. Shannon, R.K. Waring, Origin of the yellow color of complex nickel oxides, *J. Solid State Chem.* 39 (1981) 277–287, [https://doi.org/10.1016/0022-4596\(81\)90261-9](https://doi.org/10.1016/0022-4596(81)90261-9).
- [6] M.A. Ruiz-Preciado, A. Bulou, M. Makowska-Janusik, A. Gibaud, A. Morales-Acevedo, A. Kassiba, Nickel titanate (NiTiO₃) thin films: RF-sputtering synthesis and investigation of related features for photocatalysis, *CrystEngComm.* 18 (2016) 3229–3236, <https://doi.org/10.1039/C6CE00306K>.
- [7] A. Sobhani-Nasab, S.M. Hosseinpour-Mashkani, M. Salavati-Niasari, H. Taqiri, S. Bagheri, K. Saberyan, Synthesis, characterization, and photovoltaic application of NiTiO₃ nanostructures via two-step sol–gel method, *J. Mater. Sci. Mater. Electron.* 26 (2015) 5735–5742, <https://doi.org/10.1007/s10854-015-3130-0>.
- [8] Y. Absalan, I. Bratchikova, O.V. Kovalchukova, Accurate investigation to determine the best conditions for using NiTiO₃ for bromophenol blue degradation in the environment under UV–vis light based on concentration reduction and to compare it with TiO₂, *Environ. Nanotechnol. Monit. Manag.* 8 (2017) 244–253, <https://doi.org/10.1016/j.enmm.2017.08.001>.
- [9] X. Shu, J. He, D. Chen, Visible-Light-Induced Photocatalyst Based on Nickel Titanate Nanoparticles, *Ind. Eng. Chem. Res.* 47 (2008) 4750–4753, <https://doi.org/10.1021/ie071619d>.
- [10] S.B. Rawal, S. Bera, D. Lee, D.J. Jang, W.I. Lee, Design of visible-light photocatalysts by coupling of narrow bandgap semiconductors and TiO₂: effect of their relative energy band positions on the photocatalytic efficiency, *Catal. Sci. Technol.* 3 (2013) 1822, <https://doi.org/10.1039/c3cy00004d>.
- [11] R.S. Singh, T.H. Ansari, R.A. Singh, B.M. Wanklyn, Electrical conduction in NiTiO₃ single crystals, *Mater. Chem. Phys.* 40 (1995) 173–177, [https://doi.org/10.1016/0254-0584\(95\)01478-0](https://doi.org/10.1016/0254-0584(95)01478-0).
- [12] M.A. Ruiz-Preciado, A. Kassiba, A. Gibaud, A. Morales-Acevedo, Comparison of nickel titanate (NiTiO₃) powders synthesized by sol–gel and solid state reaction, *Mater. Sci. Semicond. Process.* 37 (2015) 171–178, <https://doi.org/10.1016/j.mssp.2015.02.063>.
- [13] Y.-J. Lin, Y.-H. Chang, W.-D. Yang, B.-S. Tsai, Synthesis and characterization of ilmenite NiTiO₃ and CoTiO₃ prepared by a modified Pechini method, *J. Non-Cryst. Solids.* 352 (2006) 789–794, <https://doi.org/10.1016/j.jnoncrysol.2006.02.001>.
- [14] P.S. Anjana, M.T. Sebastian, Synthesis, Characterization, and Microwave Dielectric Properties of ATiO₃ (A = Co, Mn, Ni) Ceramics, *J. Am. Ceram. Soc.* 89 (2006) 2114–2117, <https://doi.org/10.1111/j.1551-2916.2006.01004.x>.
- [15] T.M. Pan, T.F. Lei, T.S. Chao, Comparison of ultrathin CoTiO₃ and NiTiO₃ high-*k* gate dielectrics, *J. Appl. Phys.* 89 (2001) 3447–3452, <https://doi.org/10.1063/1.1347405>.
- [16] J.K. Harada, L. Balhorn, J. Hazi, M.C. Kemei, R. Seshadri, Magnetodielectric coupling in the ilmenites MTiO₃ (M = Co, Ni), *Phys. Rev. B.* 93 (2016) 104404, <https://doi.org/10.1103/PhysRevB.93.104404>.
- [17] J.E. Bratvold, H. Fjellvåg, O. Nilsen, Atomic Layer Deposition of oriented nickel titanate (NiTiO₃), *Appl. Surf. Sci.* 311 (2014) 478–483, <https://doi.org/10.1016/j.apsusc.2014.05.092>.
- [18] J.E. Bratvold, H. Fjellvåg, O. Nilsen, Phase and Orientation Control of NiTiO₃ Thin Films, *Materials (Basel)* 13 (2019) 112, <https://doi.org/10.3390/ma13010112>.
- [19] K. Yoshimatsu, H. Mashiko, N. Umezawa, K. Horiba, H. Kumigashira, A. Ohtomo, Electronic Structures and Photoanodic Properties of Ilmenite-type MTiO₃ Epitaxial Films (M = Mn, Fe, Co, Ni), *J. Phys. Chem. C.* 121 (2017) 18717–18724, <https://doi.org/10.1021/acs.jpcc.7b06076>.
- [20] J.B. Bellam, M.A. Ruiz-Preciado, M. Edely, J. Szade, A. Jouanneaux, A.H. Kassiba, Visible-light photocatalytic activity of nitrogen-doped NiTiO₃ thin films prepared by a co-sputtering process, *RSC Adv.* 5 (2015) 10551–10559, <https://doi.org/10.1039/C4RA12516A>.
- [21] J.B. Bellam, A. Jouanneaux, V. Subramaniam, A.H. Kassiba, Statistical experimental design to optimize RF-sputtered NiTiO thin films, *J. Mater. Sci. Mater. Electron.* (2020), <https://doi.org/10.1007/s10854-020-02940-8>.
- [22] A. Sediri, M. Zaghrioui, A. Barichard, C. Autret, B. Negulescu, L. Del Campo, P. Echegut, P. Laffez, Growth of polycrystalline Pr₂NiO_{4+δ} coating on alumina substrate by RF magnetron co-sputtering from composite targets, *Thin Solid Films* 600 (2016) 131–135, <https://doi.org/10.1016/j.tsf.2016.01.023>.
- [23] P. Laffez, Q. Simon, Y. Kikuchi, R. Retoux, F. Giovannelli, A. Yamamoto, Growth of polycrystalline Pr₄Ni₃O₁₀ thin films for intermediate temperature solid oxide fuel cell cathode by radio frequency magnetron co-sputtering, *Thin Solid Films* 693 (2020) 137705, <https://doi.org/10.1016/j.tsf.2019.137705>.
- [24] M. Ohring, *The Materials Science of Thin Films*, Academic Press, Boston, 1992.
- [25] C. Priestland, S.D. Hersee, The effects of pressure on the deposition rate in rf sputtering processes, *Vacuum* 22 (1972) 103–106, [https://doi.org/10.1016/0042-207X\(72\)90468-X](https://doi.org/10.1016/0042-207X(72)90468-X).
- [26] M. Salhi, S.E.K. Abaidia, S. Mammeri, B. Bouaouina, Sputter deposition of Titanium and Nickel thin films in radio frequency magnetron discharge characterized by optical emission spectroscopy and by Rutherford backscattering spectrometry, *Thin Solid Films* 629 (2017) 22–27, <https://doi.org/10.1016/j.tsf.2017.03.032>.
- [27] J.C. Helmer, C.E. Wickersham, Pressure effects in planar magnetron sputter deposition, *J. Vac. Sci. Technol. Vac. Surf. Films.* 4 (1986) 408–412, <https://doi.org/10.1116/1.573892>.
- [28] A. Anders, A structure zone diagram including plasma-based deposition and ion etching, *Thin Solid Films* 518 (2010) 4087–4090, <https://doi.org/10.1016/j.tsf.2009.10.145>.
- [29] International Centre for Diffraction Data PDF card n°00-005-0565.
- [30] International Centre for Diffraction Data PDF card n°06-046-1212.
- [31] P. Ballirano, R. Caminiti, Rietveld refinements on laboratory energy dispersive X-ray diffraction (EDXD) data, *J. Appl. Crystallogr.* 34 (2001) 757–762, <https://doi.org/10.1107/S0021889801014728>.
- [32] International Centre for Diffraction Data PDF card n°00-047-1049.
- [33] C.L. Zeng, M.C. Li, G.Q. Liu, W.T. Wu, Air Oxidation of Ni–Ti Alloys at 650–850 °C, *Oxid. Met.* 58 (2002) 171–184, <https://doi.org/10.1023/A:1016020709500>.
- [34] International Centre for Diffraction Data PDF card n°00-012-0708.
- [35] D.B. Goldman, Mechanism and Kinetics of Reactions in the System Ni–Ti–O, *J. Am. Ceram. Soc.* 66 (1983) 811–814, <https://doi.org/10.1111/j.1151-2916.1983.tb10568.x>.
- [36] F.K. Lotgering, Topotactical reactions with ferrimagnetic oxides having hexagonal crystal structures—I, *J. Inorg. Nucl. Chem.* 9 (1959) 113–123, [https://doi.org/10.1016/0022-1902\(59\)80070-1](https://doi.org/10.1016/0022-1902(59)80070-1).
- [37] L. Li, C. Zhang, Z. Yuan, Z. Liu, C. Li, Selectivity of Benzyl Hydroxamic Acid in the Flotation of Ilmenite, *Front. Chem.* 7 (2019) 886, <https://doi.org/10.3389/fchem.2019.00886>.
- [38] R.A.P. Ribeiro, J. Andrés, E. Longo, S.R. Lazaro, Magnetism and multiferroic properties at MnTiO₃ surfaces: a DFT study, *Appl. Surf. Sci.* 452 (2018) 463–472, <https://doi.org/10.1016/j.apsusc.2018.05.067>.
- [39] W. Sun, V. Agh, H. Mohseni, T.W. Scharf, J. Du, Experimental and computational studies on stacking faults in zinc titanate, *Appl. Phys. Lett.* 104 (2014) 241903, <https://doi.org/10.1063/1.4883747>.